On the application of the depth-averaged random walk method to solute transport simulations

Fan Yang[1], Dongfang Liang[1*], Xuefei Wu[2], Yang Xiao[3]

[1] Department of Engineering, University of Cambridge, Trumpington Street, Cambridge CB2 1PZ, United Kingdom

[2] School of Environment and Resource, Southwest University of Science and Technology, Sichuan, 621010, China

[3] State Key Laboratory of Hydrology-Water Resources and Hydraulic Engineering, Hohai University, Nanjing 210098, China

[*] Corresponding author

Abstract

Most of the current numerical studies on the solute transport problems relies on the mesh-based methods, and various sophisticated high-order accurate schemes have been developed to enhance the numerical stability and reduce the artificial diffusion associated with the advective transport process. This paper systematically studies the depth-averaged random walk scheme, which is a meshfree method with the merits of being highly robust and free of numerical diffusion. Firstly, the model is used to solve an instantaneous release problem in uniform flows. Its performance is examined by comparing numerical predictions with analytical solutions. Extensive parametric studies are carried out to investigate the influences of the number of particles and the size of time steps. The predictions are found to be independent of time steps but are sensitive to the particle numbers. Secondly, the model is applied to investigate the solute transport along a tidal estuary subject to extensive wetting and drying during tidal oscillations.

The flow velocities are interpolated from a flow solver, and the pollutant distributions predicted with a grid-based method are used as references. The sampling technique is further optimised, which also offers a guideline for estimating the total number of particles needed in the application. Finally, the model is applied to investigate the wind-induced chaotic mixing in a circular shallow basin. The effect of diffusion on the chaotic mixing is investigated. The advantage of the random walk model includes simplicity and little numerical diffusion. This study proposes a generic sampling method to interpret the output of the random walk method and highlights the importance of accurately taking diffusion into account in studying the mixing phenomena.

Keywords: advective diffusion, shallow water flows, pollutant transport, random walk method, numerical diffusion

1 Introduction

Pollutant transport in water bodies has been extensively studied since it is relevant to a wide range of environmental problems, which may cause significant economic losses (Rajar 1997). Among the natural water bodies, many can be described as shallow water, such as estuarine, coastal and inland flows. The horizontal scale of these flows is much larger than its depth. Therefore, it can be assumed that the solute is well-mixed vertically over the water column, allowing a depth-integrated approach to investigate the solute transport process. This paper focuses on the solute transportation in shallow water bodies specifically.

With the development of computing techniques, many modern numerical methods have been established to solve such problems (Lin & Falconer 1997; Gupta et al. 2004; Begnudelli & Sanders 2006; Benkhaldoun et al. 2007). Previously, most of the research is based on Eulerian approaches to solve the standard advection-diffusion equation using finite-difference or finite-

element techniques (Yang et al. 2018; Liang et al. 2006; Mingham et al. 2001). However, these grid-based methods have proven to be deficient in addressing steep concentration gradients and tend to produce numerical diffusion (Wu & Liang 2018). By contrast, Lagrangian methods use discrete particles as indicators to represent clouds of solute or pollutant, and these particles are tracked independently in flows. Thus, the Lagrangian approach can usually yield an accurate estimation (Zhang 2007). Nowadays, thanks to the dramatic progress in the quality and speed of computers, the computational price for the Lagrangian approach could be well paid. Its merits, such as conservative and free from artificial diffusion, become more and more outstanding. Compared with Euler methods, the Lagrangian methods are better suited to the simulation of complex phenomena, where high contamination gradients are involved.

The computational cost for Lagrangian approaches depends on two factors: the number of particles to present the pollutant cloud, and the size of the computational time step that the model applied. The choice of these two factors is crucial to the efficiency of the random walk model. It is necessary to manually tune the number of particles and the size of time steps. Firstly, an ideal case is used to investigate the sensitivity of numerical solutions to the time steps and particle numbers in the depth-averaged random walk model. Then, the model is used to solve a solute oscillation problem along a hypothetical tidal estuary. The results of a TVD-MacCormack model are used as a reference. Finally, the paper describes the applications of the random walk scheme to simulate the wind-driven chaotic mixing in a shallow circle lake. The results are compared with previous research from a qualitative point of view.

2 Depth-averaged Advection-diffusion equation

The governing equation of solute transportation in water bodies is the advection-diffusion equation (Gresho & Sani 1998). Advection is the transportation of a substance by a fluid due to the fluid's bulk motion. In this process, it is assumed that particles of the solute exactly follow the shallow flow. Diffusion is the process whereby solute transports from higher

concentration to lower concentration in flow due to random movements. It is assumed that the diffusive substances would not affect the motion of flows. In other words, the flow field is independent of the existence of the diffusive materials. With these assumptions, the conservation of solute mass is presented as:

$$\frac{\partial(sh)}{\partial t}+\frac{\partial(ush)}{\partial x}+\frac{\partial(vsh)}{\partial y}=\frac{\partial}{\partial x}\left(dD_{xx}\frac{\partial s}{\partial x}+dD_{xy}\frac{\partial s}{\partial y}\right)+\frac{\partial}{\partial y}\left(dD_{yx}\frac{\partial s}{\partial x}+dD_{yy}\frac{\partial s}{\partial y}\right)+q_s \quad (1)$$

where t is time; s is the depth-averaged concentration of the solute; h is the water depth; u and v represent the velocities along x and y-axis respectively; q_s is the sources term of the governing equation, representing the increase ($q_s > 0$) or decrease ($q_s < 0$) in the total amount of the solute; D_{xx}, D_{xy}, D_{yx} and D_{yy} represent the dispersion-diffusion tensor of depth-averaged mixing in Cartesian coordinates. The relationship between the streamwise-transverse system and Cartesian coordinate can be expressed as:

$$D_{xx}=D_s\cos^2\theta+D_t\sin^2\theta \quad (2)$$

$$D_{xy}=D_{yx}=(D_s-D_t)\sin\theta\cos\theta \quad (3)$$

$$D_{yy}=D_s\sin^2\theta+D_t\cos^2\theta \quad (4)$$

where $D_s=\varepsilon_s du_*$, $D_t=\varepsilon_t du_*$ (5)

D_s and D_t are the streamwise and transverse diffusion coefficients; ε_s and ε_t are two dimensionless constants representing streamwise dispersion and transverse diffusion respectively. $\theta = arctan(\, v/u\,)$ is the angle between the direction along the x-axis and the direction of the local flow. The shear velocity u_* is expressed as Eq. (6) using Chézy coefficient.

$$u_*=\frac{\sqrt{g}}{Ch\acute{e}zy}\cdot\sqrt{u^2+v^2} \quad (6)$$

3 Depth-averaged random-walk method

3.1 Equation reformation

In this paper, the depth-averaged advection-diffusion equation is recast in a new form that utilises a consistent particle-tracking algorithm. A new concentration variable, $S = sh$. is introduced. Then, the new form of the equation can be written as:

$$\frac{\partial S}{\partial t}+\frac{\partial (US)}{\partial x}+\frac{\partial (VS)}{\partial y}=\frac{\partial^2 (D_{xx}S)}{\partial x^2}+2\frac{\partial^2 (D_{xy}S)}{\partial x \partial y}+\frac{\partial^2 (D_{yy}S)}{\partial y^2} \tag{7}$$

$$U = u+\frac{\partial D_{xx}}{\partial x}+\frac{\partial D_{xy}}{\partial y}+\frac{D_{xx}}{h}\frac{\partial h}{\partial x}+\frac{D_{xy}}{h}\frac{\partial h}{\partial y} \tag{8}$$

$$V = v+\frac{\partial D_{yy}}{\partial y}+\frac{\partial D_{xy}}{\partial x}+\frac{D_{yy}}{h}\frac{\partial h}{\partial y}+\frac{D_{xy}}{h}\frac{\partial h}{\partial x} \tag{9}$$

The source term q_s in the previous equation is neglected in the new form. S is considered as a probability density function. U and V in the Eqs. (8) and (9) represent the modified advective velocities. The more detailed explanations of this scheme can be found in Wu & Liang (2018). This depth-averaged random walk model is then performed by advection and diffusion transport process for each time step in the following content.

3.2 Advective transport

In the advective transport, the assumption is that particles exactly follow the flows. However, most of the input data for the flow field is firstly solved by traditional grid-based methods. The advective velocities in Eqs. (8) and (9) are necessary to be evaluated at each position of particles. In each grid cell that contains the particle, the velocities u and v are interpolated to

the second-order accuracy. The new particle position after the advective transport process can be expressed as Eqs. (10) and (11) using the second-order accurate iterative technique:

$$x^a = x^{old} + \bar{U}\Delta t \tag{10}$$

$$y^a = y^{old} + \bar{V}\Delta t \tag{11}$$

where $\bar{U}$ and $\bar{V}$ are the flow velocity used in calculating the particles' advective displacement in each time step. To increase the order of accuracy, they are taken to be the time-averaged velocity within each time step.

$$\bar{U} = \frac{1}{2}(U(x^{old}, y^{old}, t) + U(x^a, y^a, t + \Delta t)) \tag{12}$$

$$\bar{V} = \frac{1}{2}(V(x^{old}, y^{old}, t) + V(x^a, y^a, t + \Delta t)) \tag{13}$$

3.3 Diffusive transport

After the advection process, the particles undergo diffusion transport in a time step. The random streamwise and transverse velocities are calculated as:

$$U_s^d = r_s\sqrt{\frac{2D_s}{\Delta t}} \tag{14}$$

$$V_t^d = r_t\sqrt{\frac{2D_t}{\Delta t}} \tag{15}$$

The random numbers r_s and r_t are independent and follow a normal distribution with a mean of zero and a standard deviation of unity. The subscripts *s* and *t* represent the streamwise and transverse direction, respectively. The superscript *d* represents the diffusion-related velocity components. In the Cartesian coordinate system, the diffusion-related velocity components are expressed as:

$$U_x^d = U_s^d \cos\theta - V_t^d \sin\theta \quad (16)$$

$$V_y^d = U_s^d \sin\theta + V_t^d \cos\theta \quad (17)$$

Finally, particle's new coordinates after one-time step can be evaluated as:

$$x^{new} = x^a + U_x^d \Delta t \quad (18)$$

$$y^{new} = y^a + V_y^d \Delta t \quad (19)$$

3.4 Boundary condition

Particles follow a "random walk" trajectory with the flow inside the computational domain. The boundary treatment is designed to prevent them from crossing solid boundaries. In this study, the fully reflective boundary condition is applied to particles that penetrate the solid boundaries after implementing Eqs. (18) and (19). When the time step is not large, such a treatment then reflects the particles back into the computational domain.

4 Advection and diffusion transport in uniform flows

The instantaneous release problem in uniform flows is tested firstly using the random walk model. When the uniform flow only follows the x-axis ($v = 0$, $D_{xy} = 0$, $D_{xx} = D_s$, $D_{yy} = D_t$), the analytical solution of this ideal test case can be expressed as:

$$s(x,y,t) = \frac{\frac{M}{h}}{4\pi t\sqrt{D_s D_t}} e^{-\frac{(x-x_0-ut)^2}{4D_s t} - \frac{(y-y_0)^2}{4D_t t}} \quad (20)$$

In this section, the total amount of solute material M = 233.06 kg is released suddenly at the initial location (x_0, y_0). As shown in Figure 1, the water depth is set to be h = 1 m, and the *Chézy* coefficient is 40 $m^{1/2}/s$ for the whole test area. The streamwise dispersion and transverse diffusion are typical values of 13.0 and 1.2 respectively for open channel flows (Falconer 1991).

Two flow conditions are considered in this section. The first one is a uniform flow with $u = 1$ m/s along the x-axis ($\theta = 0$). The solute material is initially located at $(x_0, y_0) = (0, 400\text{ m})$. The second one is a uniform flow aligned diagonal direction ($\theta = 45^\circ$). The velocity is set to be $u = v = 1/\sqrt{2}$ m/s. For computations in both scenarios, the particle numbers P is 2.33×10^6 and the time step is 1 s.

Figure 1 The instantaneous release problem in a uniform flow

(a) x-direction flow; (b) diagonal-direction flow

The development of concentration contours for flows in the x-axis direction and diagonal direction are presented in Figures 1 (a) and (b) respectively. It is notable that the major axis of the ellipses patches is along their flow directions. The cloud of the solute experienced rapid elongation on its path. The reason is that streamwise dispersion is ten times larger than the transverse diffusion. The results for the same test case obtained by a grid-based method, TVD-MacCormack, can be found in Liang et al. (2010).

4.1 The influence of time steps

The advantage of the random walk model includes high accuracy and small numerical diffusion. However, the expense that comes with this Lagrangian approach is its high computational cost. As seen in the scheme description, the amount of the computation depends on two factors: the size of the computational time steps the model applied, and the number of particles to present the pollutant cloud. Therefore, the choices of these two factors are crucial to the efficiency of the random walk model. The following part of this section is to discuss the influence of the two parameters on the random walk model when applied to the instantaneous release problem in uniform flows.

Figure 2 Concentration distributions at 600 s with changes in time steps (*x*-direction flow)

Figure 3 Development of peak concentrations with changes in time steps (*x*-direction flow)

A great deal of research on time steps has been taken under the Euler scheme. The size of Δt is restricted by the Courant-Friedrichs-Lewy condition. Usually, the smaller the time step is, the more accurate and stable the simulation will be. However, it tells a different story for the random walk model. Figure 2 presents the longitudinal concentration profile at 600 s after the solute release. Regardless of the time step of 600 s or 0.01 s, the same concentration profile is predicted by the model. Variations of the peak concentration are not affected by the size of time steps as well, as seen in Figure 3.

This independent property of time steps can be derived through the iteration process. After *n* times iterations, the position of the particles at *t* time is expressed as:

$$x_1(t) = x_0 + \bar{U}n\Delta t + \sqrt{2D_s\Delta t} \cdot \sum_{i=1}^{n} r_i \tag{21}$$

$$y_1(t) = y_0 + \bar{V}n\Delta t + \sqrt{2D_t\Delta t} \cdot \sum_{j=1}^{n} r_j \tag{22}$$

If the time step changes to be $m\Delta t$, *n/m* times iterations are needed for the new time step. Then, the new position of the particles at *t* time is expressed as:

$$x_2(t) = x_0 + \bar{U}n\Delta t + \sqrt{2D_s\Delta t} \cdot \sqrt{m} \sum_{i=1}^{n/m} r_i \tag{23}$$

$$y_2(t) = y_0 + \bar{V}n\Delta t + \sqrt{2D_t\Delta t} \cdot \sqrt{m} \sum_{j=1}^{n/m} r_j \tag{24}$$

In the present model, the random numbers r_i follow a normal distribution with a mean of zero and a standard deviation of unity, as shown in Eq. (25). According to properties of a normal distribution (Bryc, Wlodzimierz 1995), $\sum_{i=1}^{n} r_i$ and $\sqrt{m} \sum_{j=1}^{n/m} r_j$ have the same expectation and deviation.

$r_i \sim N(\mu, \sigma^2)$, where $\mu = 0, \sigma^2 = 1$ (25)

$$\sum_{i=1}^{n} r_i \sim N(n\mu, n\sigma^2) \quad (26)$$

$$\sqrt{m} \cdot \sum_{j=1}^{\frac{n}{m}} r_j \sim N\left(\sqrt{m}\frac{n}{m}\mu, \frac{n}{m}\left(\sqrt{m}\sigma\right)^2\right) \quad (27)$$

Therefore, the results will all obey the distribution of $N(0, n)$ no matter what size of the time step is used. It can be concluded that the change of time steps does not affect the accuracy of the present model for the uniform flow with constant water depth.

4.2 The influence of particle numbers

Figure4 shows a qualitative illustration of the solute transport process predicted by the random walk model using different configurations of particle numbers. In general, the contour turns out to be more notable with the particle number increases. Larger particle numbers significantly improve the visual effect of the elliptical cloud for solute distribution.

Figure 4 Evolution of the solute cloud in *x*-direction uniform flows (P_0 = 233)

Figure 5 Variation of peak concentration for *x*-direction flows

Figure 6 Relative errors of peak concentration (a) with the changes in particle numbers in each sampling bins; (b) with changes in time

To get a quantitative analyse, the predicted results are compared with analytical solutions. Figure 5 shows variations of peak concentration with different particle numbers used in the simulation. The size of sampling bins is set to be a circle with a radius of one meter. It is notable that small particle numbers tend to produce numerical oscillations. On the contrary, by setting a more substantial number of particles in the model, the prediction approaches closer to the

analytical solution. For example, when 2.33×10^7 particles simulated in the model, the peak concentration is identical with the analytical solution. The relative errors with different particle numbers different bin sizes are compared in Figure 6 (a). In the legend, *r* represents the radius of the bin. It is clear that with the growth of particle number put into the simulation, the error decreases significantly. The error for small particle numbers jumps beyond 18%, which is unacceptable in a strict simulation. When the number of particles in each sampling bins approaches 200 to 300, the relative error is reduced to less than 5%. This means that the particle should be guaranteed to be higher than hundreds per bin to show a reasonable result for the solute concentration. Also, it is worth to note that the error for both x-direction and diagonal flows is always consistent with each other, as shown in Figure 6 (b). This means the model is not affected by the concentration gradient.

5 Solute oscillation along a one-dimensional tidal estuary

This section considers solute material is transported forward and backward in a hypothetical tidal estuary. As shown in Figure 7, the boundary condition for the left end is regarded as a sinusoidal tide, while the right side of this estuary is considered as a vertical wall. The total length of the estuary is 13,800 m, and the altitude changes from -5 m at the end of the seaward to 0 m at the right end. In this case, the tidal flow has an average water level of 0 m and amplitude of 2 m, rising from the average water level at the beginning of the simulation. Before the pollutant transport simulation, the predictions of the flow field were obtained by using TVD-MacCormack scheme to solve the SWEs (shallow water equations). Detailed information can be found in Liang et al. (2010). The discretized velocity field is then reconstructed into a continuous form using linear interpolation.

Figure 7 One-dimensional hypothetical tidal estuary

The initial concentration is set to be 100 units at the cell located at x = 10 km, while the concentration of the remaining fields is set to be zero. An illustration for the particles position and their distribution along time is given by Figure 8. It is well presented that particles travel with wave flows and disperse in the longitudinal direction. The instantaneously released solute flows with the rising water to the closed wall under the influence of tidal currents, while the receding water is flowing to the open boundary. At the same time, the region of the solute is enlarging because of the effect of dispersion.

Figure 8 Distribution of solute particles along the one-dimensional hypothetical estuary

Figure 9 Distribution of the concentration along the one-dimensional hypothetical estuary

The aforementioned sampling algorithm is required to convert the scatter of particles, as illustrated in Fig. 8, to the concentration profile, as illustrated in Figure 9. This sampling algorithm is crucial in the interpretation of the results of the random walk method and in the evaluation of the concentrations. Traditionally, this concentration profile, i.e. histogram, uses a fixed length to separate different bins. However, this fixed setting may lose the accuracy at some local parts. In this work, the length of the bin is chosen automatically by including 200 particles within each bin along the hypothetical estuary. This dynamic determination of the bin size is found to avoid spurious fluctuations and achieve good comparisons with analytical and previous results. A series of smooth concentration profiles along the estuary at both high and low water levels are shown in Figure 9. When the solute cloud moves nearly to the landward position, the tidal flow generally decelerates because of the wall boundary. It is notable that the peak concentration is even higher at 27 hours than at 9 hours, as the water level is higher near the right-side wall.

Figure 10 Distribution of the concentration along the estuary with the changes in grid size. (a)3 hours; (b)9 hours; (c)27 hours; (d)33 hours; (e)51 hours

The numerical solution of TVD-MacCormack model is used as a reference for this case. For such grid-based methods, solutions are usually sensitive to its grid size. The finer the grid is, the more accurate the simulation will be, although the more computationally expensive it might be. The numerical diffusion for the Eulerian model is more obvious at the beginning because of the sharp concentration gradient. Taking Figure 10 (a) as an example, it presents the concentration profile at 3 hours since the beginning. Several different cell sizes, from 3 m to 270 m, are used in the mesh method simulation. When the mesh size is increased to 270 m, the concentration distribution is too flat to demonstrate a proper concentration distribution. The results for the grid size of 3 m are nearly three times that of 90 m. On the contrary, the random walk model is less diffusive. A narrower distribution and a higher peak concentration are predicted by the present model, and it is identical to the extreme of the concentration trend.

6 Wind-driven chaotic mixing in a shallow circle lake

In this section, the random walk model is applied to simulate the particle motion due to wind-driven mixing in a shallow lake. As shown in Figure 11, the property of the circular lake is suggested by Kranenburg (1992). The velocity field is described by a stream function in the polar coordinate system:

$$\psi = Br(1-\frac{r}{R})\sin(\phi-\theta) \text{ , where } B=\frac{\ln Z}{4\kappa}u_* H \text{ , } Z=\frac{H}{z_0} \tag{28}$$

The von Kármán constant κ is set to be 0.4; the mean depth H is 0.5m and the radius of the lake R_0 is 120 m; z_0 is a roughness height of the bed, set to 2.8 mm. The water depth h is described by a function of radial distance r from the basin centre as following:

$$h = H\left(\frac{1}{2} + \sqrt{\frac{1}{2} - \frac{1}{2}\frac{r}{R_0}}\right) \quad (29)$$

These physical parameters are set to be the same as those in Kranenburg (1992) for the comparison purpose.

Figure 11 Aerial view of the model lake with a periodic sequence of storm events

Kranenburg (1992) found that the particle motion becomes chaotic when surface wind stress periodically changes its direction. Therefore, a sequence of periodic storm events is designed for this case. During the first and second halves of a period, the direction of the storm wind jumps back and forth between the northeast and northwest directions, respectively. It is assumed that the wind stress suddenly changes its direction in between the half intervals, while its intensity is constant. At the same time, the Euler velocity field instantaneously adapts to wind conditions. The resulting flow field is governed by a dimensionless storm duration parameter μ as following:

$$\mu = \frac{\ln Z}{8\kappa R_0} u_* t_s \quad (30)$$

where t_s is the storm duration, i.e. half of the period T. For all the cases considered, Poincaré sections are used to illustrate the mixing properties, which is the superposition of particle trajectories at the end of each cycle.

Figure 12 Poincaré sections for wind periodically blowing from north-east and north-west with different μ (without diffusive process)

For comparison purposes, the diffusive process is ignored to test the behaviour of the advection part in the random walk model. These particles are tracked for 500 periods in this section. For

small μ, as shown in Figure 12 (a), the elliptic periodic points are surrounded by two large islands of regular motion. The area of the chaotic region increases with the increase of μ, while the sizes of the period-one islands decrease. When μ is beyond 0.70, the period-one elliptic points are no longer obvious, and only chaotic motion remains (for μ = 0.84). These findings are consistent with previous results of Kranenburg (1992).

Figure 13 Poincaré sections for both advection and diffusion processes with different ε_s (μ = 0.14)

Then, both advection and diffusion processes are considered as tracer particles are also spread by turbulence and shear dispersion during each storm. Figure 13 depicts the impact of streamwise dispersion ε_s (the transverse diffusion ε_t is constant at 0 in this section.) on this chaotic mixing phenomenon. For ε_s equal to 0.001, it is still clear that the circular lake is divided into two large islands and positions of the elliptic periodic points are still obvious. With the increase of the streamwise dispersion, this pattern becomes more and more blurred until the KAM (Kolmogorov-Arnold-Moser) (Kranenburg 1992) curves are no longer exits ($\varepsilon_s >$ 0.1). It is worth to mention that, the growth of the streamwise dispersion will not change the position of elliptic periodic points, but it will amplify the erratic motion considerably.

Figure 14 Poincaré sections for both advection and diffusion processes (μ = 0.28)

Figure 15 Poincaré sections for both advection and diffusion processes (μ = 0.42)

Figure 16 Snapshot of the particle distribution in Kranenburg's model lake (t = 32T; μ = 0.28)

For μ = 0.28 and 0.42, the entire calculation domain is chaotic when the dispersion ε_s is only 0.1, as shown in Figures 14 and 15. This means that the increase in the duration of the periodic

storm will exacerbate the impact of the diffusion coefficient, making it easier to achieve a chaotic state. Figure 16 shows the advection and diffusion behaviour of a line of 10,000 particles after 32 periods of the storm event. The line is initially positioned along the x-axis. Both whorl-type and tendrils structures coexist when μ is 0.28. With the increase of the dispersion parameter, elliptic and hyperbolic points all disappear, and particle motions reach the global chaotic state.

7 Conclusions

The traditional random walk model has been extended to solve the depth-integrated advection-diffusion equation. Firstly, this model is verified by solving an instantaneous release problem in uniform flows. Analytical solutions are used as a reference. The results reveal several merits of this model, including high accuracy and simplicity. Extensive parametric studies have been carried out to investigate the sensitivity of the predictions to the computational parameters. It has been found that simulations are independent of the size of the time step. The particle number significantly influences the performance of the random walk model. Too few particles degrade the visual inspection and quantitative examination of the solute distribution. In uniform-flow applications, a relatively large time step will reduce the computation expense without compromising accuracy, while particle numbers used should be chosen so that there are at least 200-300 particles in each sampling bin. Then, investigations are carried out regarding the oscillation of a pollutant cloud in a tide estuary. The sampling method is optimised to convert the particle distributions into concentration profiles. The random walk simulations display high accuracy, which can only be achieved by the method-based simulations with extremely fine resolutions. The mesh-based methods are shown to be highly sensitive to the grid resolution. Finally, the model is used to simulate the chaotic mixing process. The results for pure advection process are consistent with the findings reported in previous researches. Because of the presence of turbulent diffusion and bottom friction in any real lake,

the advection process is always accompanied by the longitudinal dispersion process. This study shows that the streamwise dispersion plays an important role in the material mixing pattern.

In summary, this study demonstrates that the random-walk model is highly stable and free of artificial diffusion in solving the solute transport problems in aquatic environments. In particular, this study proposes a generic sampling technique to convert the scatter of discrete particles into the solute concentration, which can also be used for estimating the total number of particles needed for the simulation.

8 Acknowledgements

We are grateful for financial support provided by the Royal Academy of Engineering UK-China Urban Flooding Research Impact Programme (UUFRIP\100051), the 111 Project (B17015) and the China Scholarship Council (CSC, No.201708060090).

References

Begnudelli L, Sanders B F. 2006 Unstructured grid finite-volume algorithm for shallow-water flow and scalar transport with wetting and drying. *Journal of hydraulic engineering*, 132(4): 371-384.

Benkhaldoun F, Elmahi I, Seaı M. 2007 Well-balanced finite volume schemes for pollutant transport by shallow water equations on unstructured meshes. *Journal of computational physics*, 226(1): 180-203.

Bryc, W. 2012 The normal distribution: characterizations with applications. Springer Science & Business Media.

Falconer, R. A. 1991 Review of modelling flow and pollutant transport processes in hydraulic basins. In *Water pollution: Modelling, measuring and prediction.* Springer, Dordrecht. pp. 3-23

Gresho P M, Sani R L. 1998 Incompressible flow and the finite element method. Volume 1: Advection-diffusion and isothermal laminar flow. United States.

Gupta, I., Dhage, S., Chandorkar, A. A., & Srivastav, A. 2004 Numerical modeling for Thane creek. *Environmental Modelling & Software*, 19(6), 571-579.

Kranenburg, C. 1992 Wind-driven chaotic advection in a shallow model lake. *Journal of hydraulic research*, 30(1), 29-46.

Liang, D., Falconer, R. A., & Lin, B. 2006 Comparison between TVD-MacCormack and ADI-type solvers of the shallow water equations. *Advances in water resources*, 29(12), 1833-1845.

Liang, D., Wang, X., Falconer, R. A., & Bockelmann-Evans, B. N. 2010 Solving the depth-integrated solute transport equation with a TVD-MacCormack scheme. *Environmental Modelling & Software*, 25(12), 1619-1629.

Lin, B., & Falconer, R. A. 1997 Tidal flow and transport modeling using ULTIMATE QUICKEST scheme. *Journal of hydraulic engineering*, 123(4), 303-314.

Mingham, C. G., Causon, D. M., & Ingram, D. M. 2001 A TVD MacCormack scheme for transcritical flow. *In Proceedings of the Institution of Civil Engineers-Water and Maritime Engineering*. Thomas Telford Ltd. 148(3): 167-175.

Rajar, R. (1997). The role of mathematical models, physical models and field measurements in water pollution problems Vol. 20. WIT Press.

Wu, X. F., & Liang, D. 2018 Study of Pollutant Transport in Depth-averaged Flows using Random Walk Method. *Journal of Hydrodynamics*, 2018: 1-13.

Wu, X. F., Yang, F., & Liang, D. F. 2018 Study of Pollutant Transport in Environmental Flows Using Depth-Averaged Random Walk Method. EPiC Series in Engineering, 2018(3): 2342--2350

Yang, F., Liang, D., & Xiao, Y. 2018 Influence of Boussinesq coefficient on depth-averaged modelling of rapid flows. *Journal of Hydrology*, 559, 909–919.

Zhang, Z. and Chen, Q., 2007 Comparison of the Eulerian and Lagrangian methods for predicting particle transport in enclosed spaces. *Atmospheric Environment*, 41(25), pp.5236-5248.

Figure

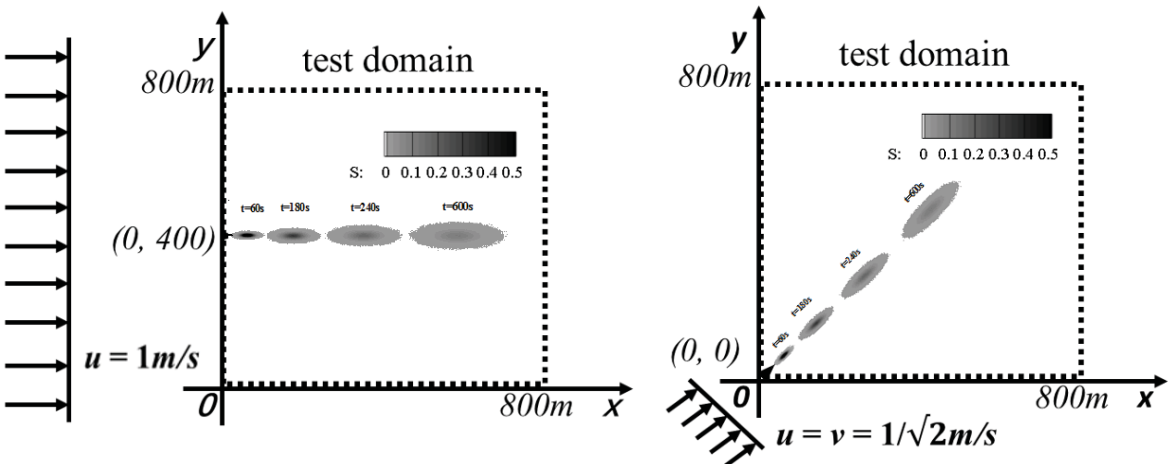

Figure 1 The instantaneous release problem in a uniform flow
(a) x-direction flow; (b) diagonal-direction flow

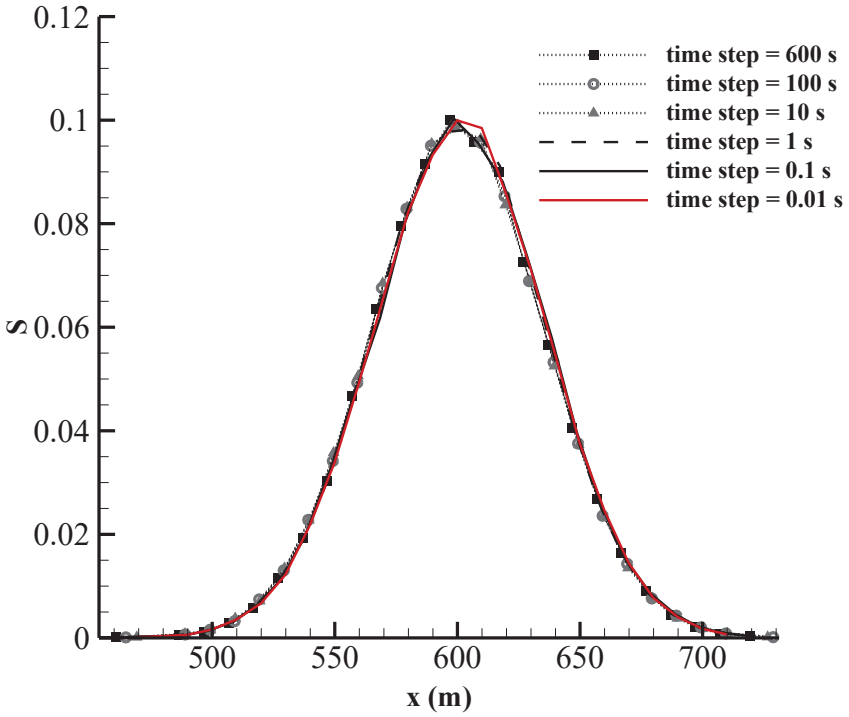

Figure 2 Concentration distributions at 600s with changes in time steps (*x*-direction flow)

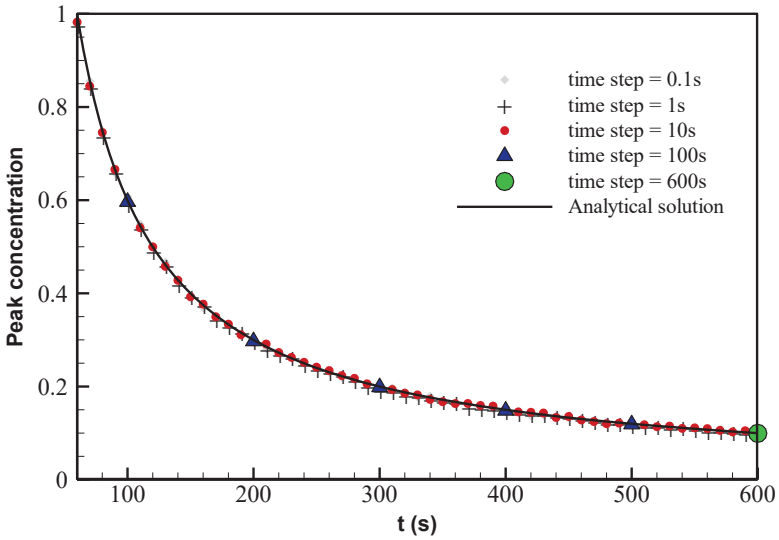

Figure 3 Development of peak concentrations with changes in time steps (*x*-direction flow)

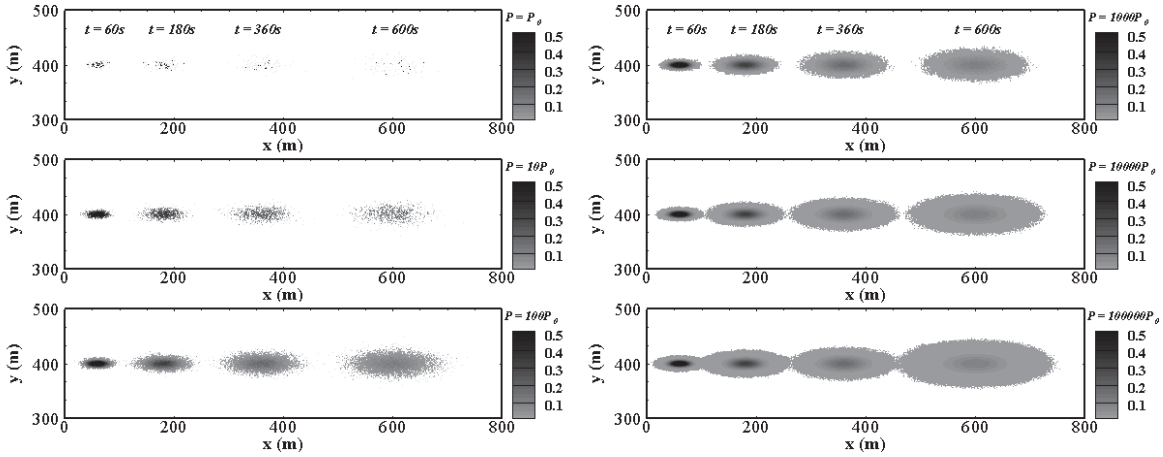

Figure 4 Evolution of the solute cloud in *x*-direction uniform flows (P_0 = 233)

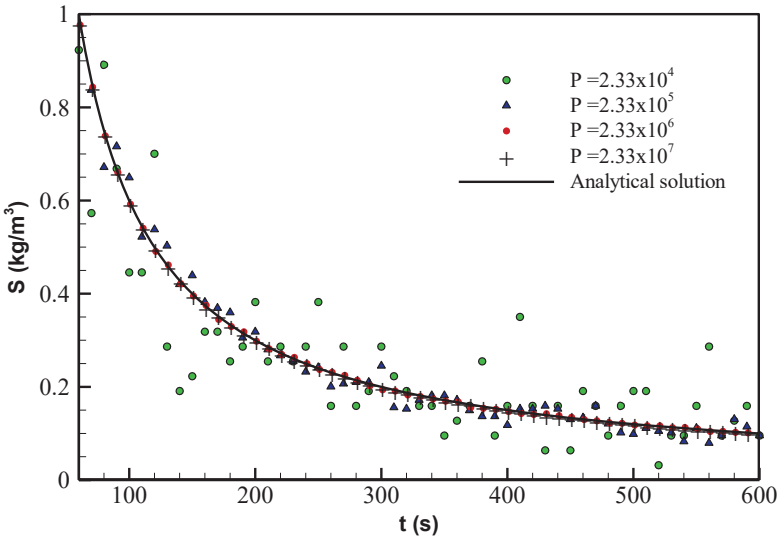

Figure 5 Variation of peak concentration for *x*-direction flows

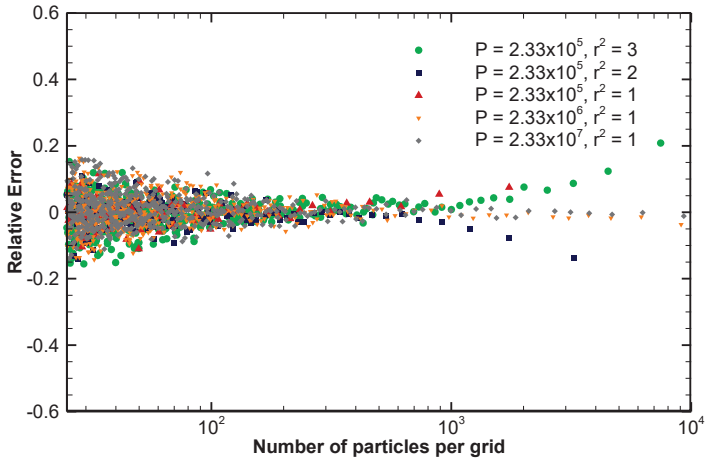

(a)

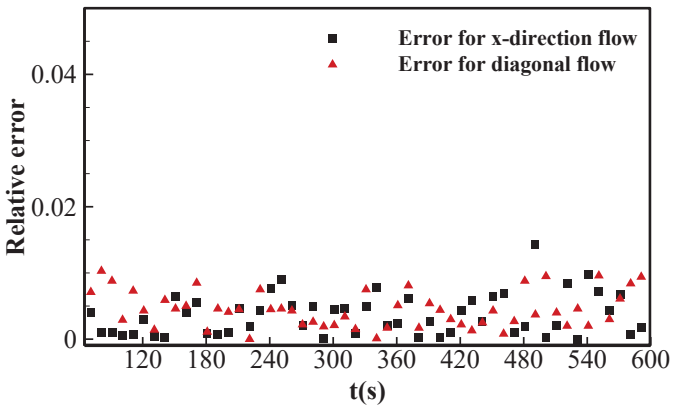

(b)

Figure 6 Relative errors of peak concentration (a)with the changes in particle numbers in each sampling bins; (b) with changes in time

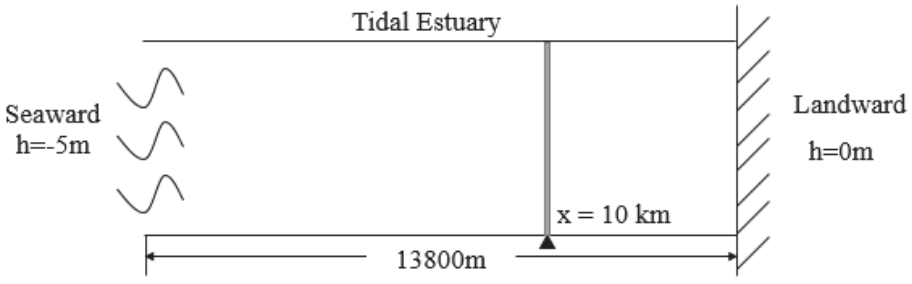

Figure 7 One-dimensional hypothetical tidal estuary

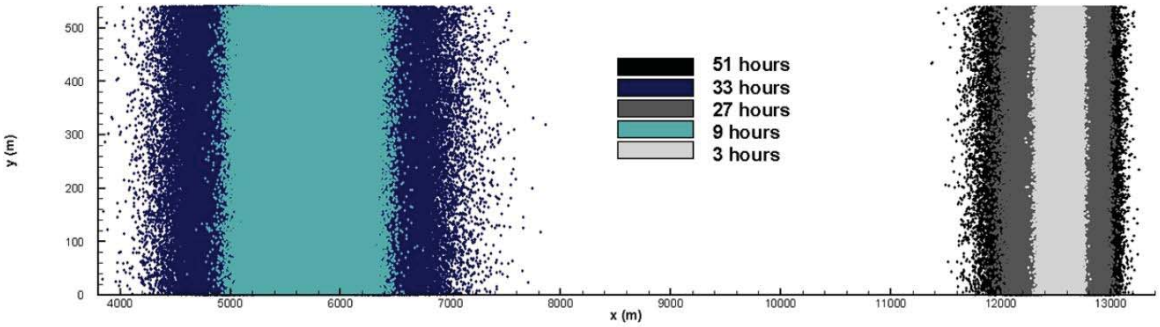

Figure 8 Distribution of solute particles along the one-dimensional hypothetical estuary

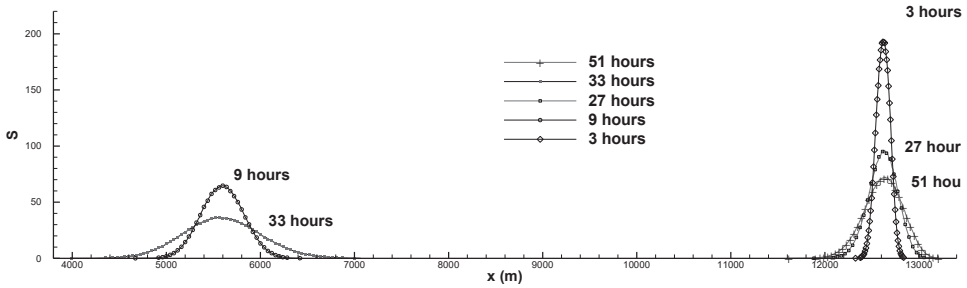

Figure 9 Distribution of the concentration along the one-dimensional hypothetical estuary

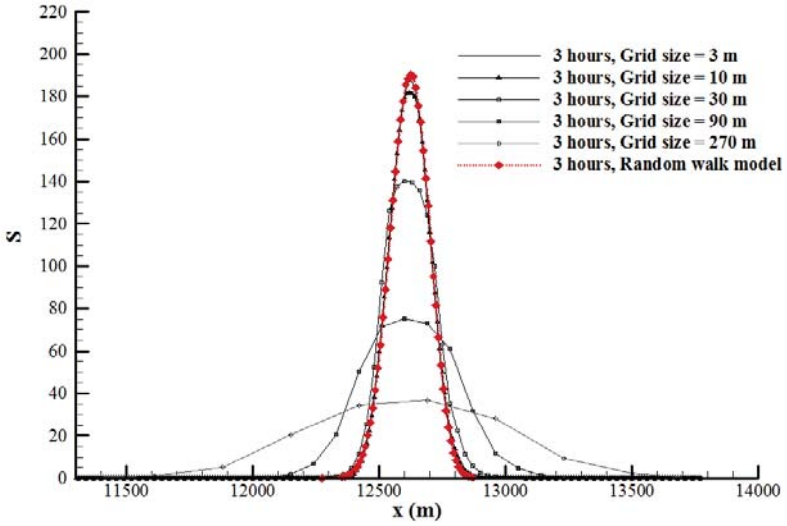

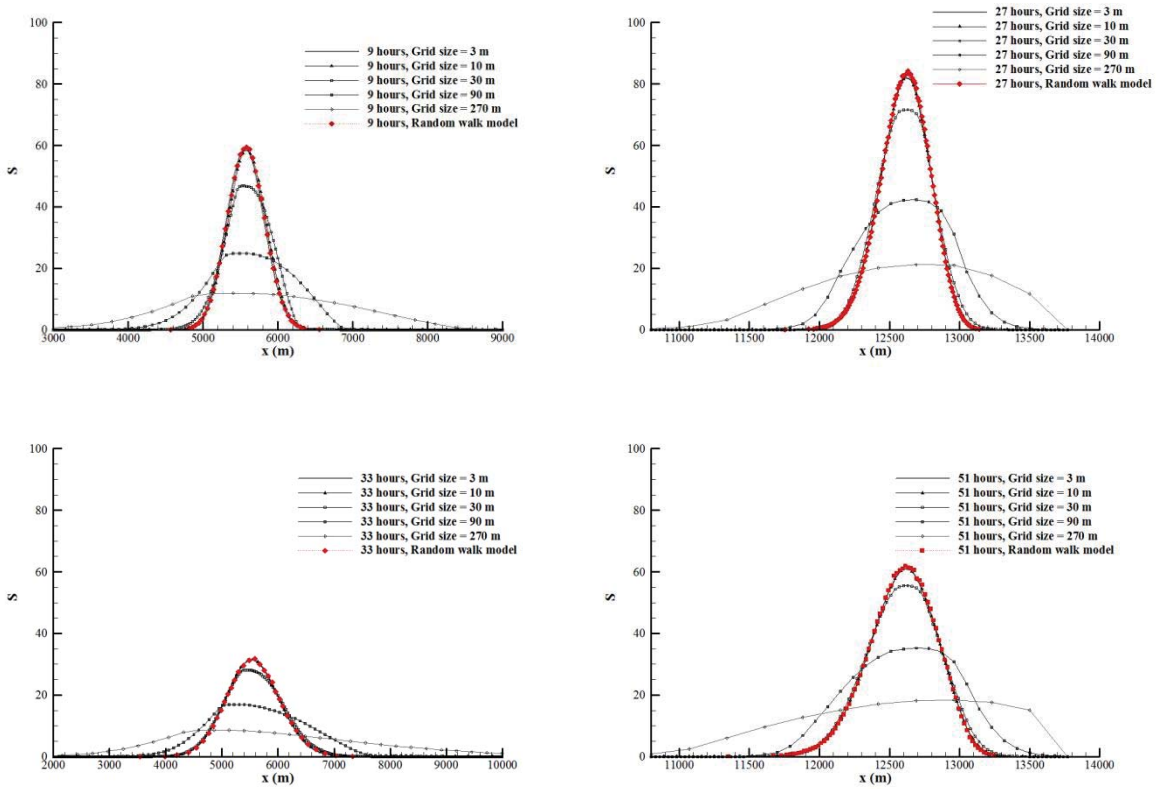

Figure 10 Distribution of the concentration along the estuary with the changes in grid size. (a)3 hours; (b)9 hours; (c)27 hours; (d)33 hours; (e)51 hours

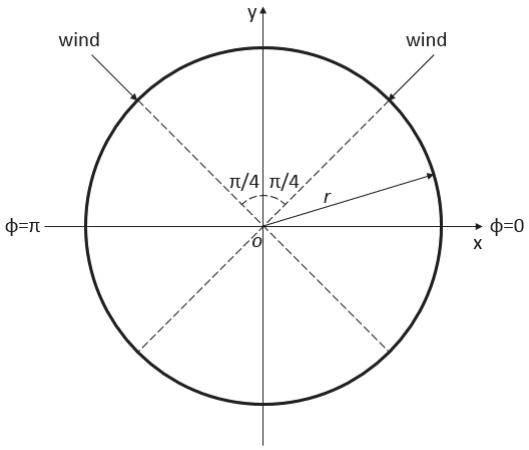

Figure 11 Aerial view of the model lake with a periodic sequence of storm events

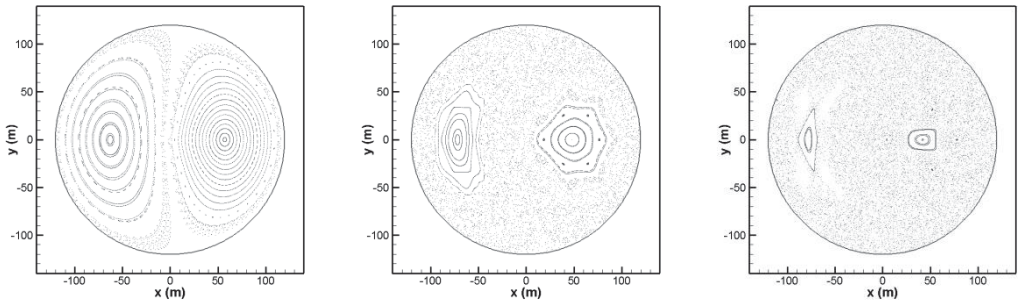

(a) $\mu = 0.14$ (b) $\mu = 0.28$ (c) $\mu = 0.42$

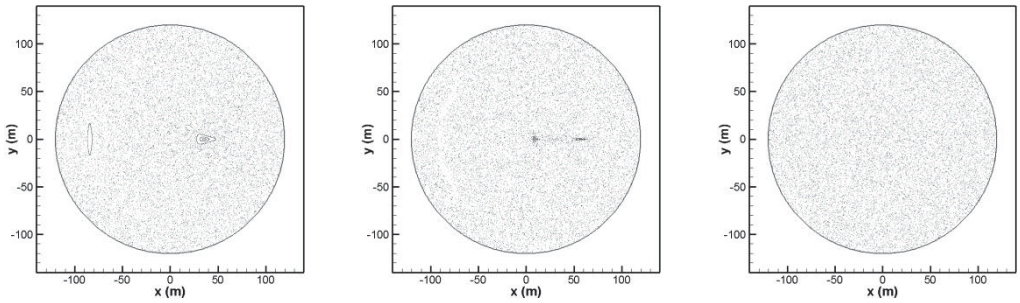

(e) $\mu = 0.56$ (f) $\mu = 0.70$ (g) $\mu = 0.84$

Figure 12 Poincaré sections for wind periodically blowing from north-east and north-west with different μ (without diffusive process)

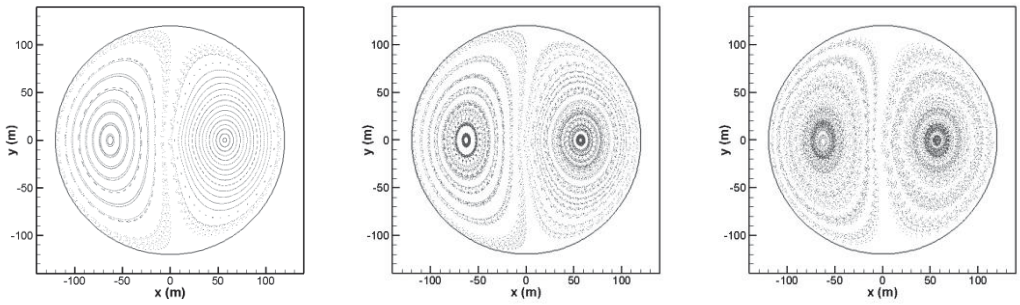

(a) $\varepsilon_s = 0.0$ (b) $\varepsilon_s = 0.001$ (c) $\varepsilon_s = 0.01$

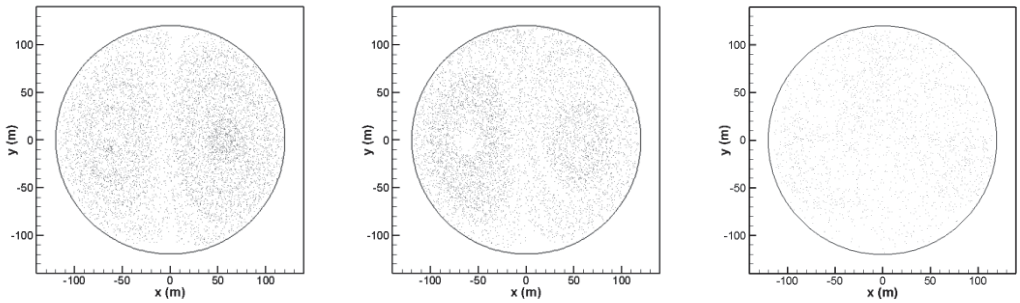

(e) $\varepsilon_s = 0.1$ (f) $\varepsilon_s = 1$ (g) $\varepsilon_s = 10$

Figure 13 Poincaré sections for both advection and diffusion processes with different ε_s (μ = 0.14)

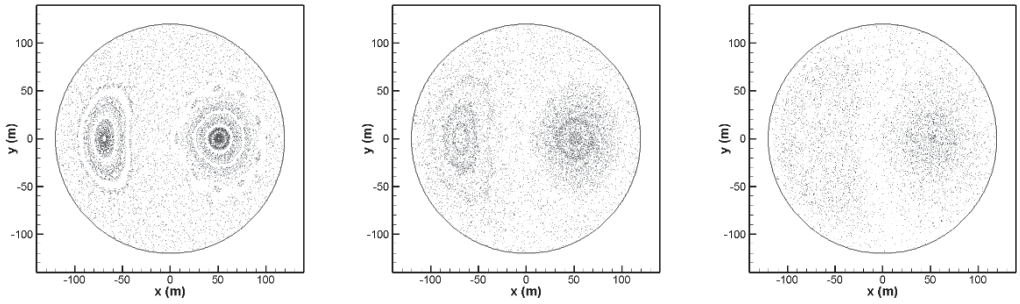

(a) $\varepsilon_s = 0.001$ (b) $\varepsilon_s = 0.01$ (c) $\varepsilon_s = 0.1$

Figure 14 Poincaré sections for both advection and diffusion processes (μ = 0.28)

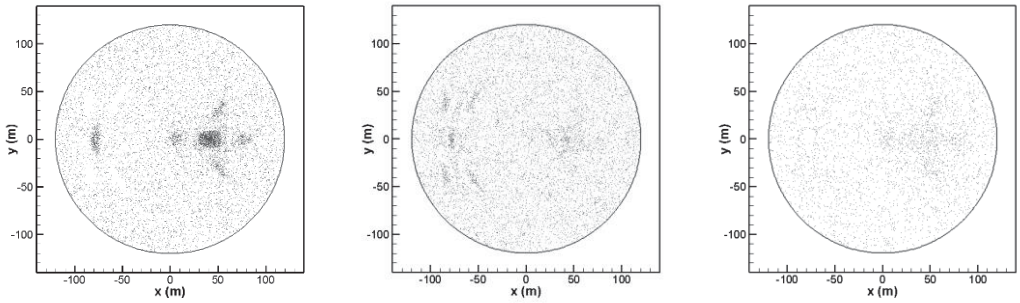

(a) ε_s = 0.001 (b) ε_s = 0.01 (c) ε_s = 0.1

Figure 15 Poincaré sections for both advection and diffusion processes (μ = 0.42)

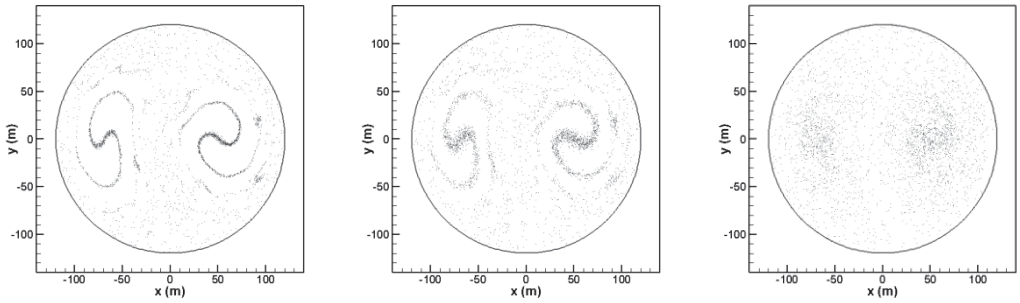

(a) ε_s = 0.001 (b) ε_s = 0.01 (c) ε_s = 0.1

Figure 16 Snapshots of the particle distribution in Kranenburg's model lake (t = 32T; μ = 0.28)